ISSN 1062-8738, Bulletin of the Russian Academy of Sciences: Physics, 2018, Vol. 82, No. 6, pp. 654–660. © Allerton Press, Inc., 2018.

Solution of Quantum Mechanical Problems Using Finite Element Method and Parametric Basis Functions[1]

O. Chuluunbaatar[a, b], S. I. Vinitsky[a, c, *], A. A. Gusev[a], V. L. Derbov[d], and P. M. Krassovitskiy[a, e]

[a] *Joint Institute for Nuclear Research, Dubna, 141980 Russia*
[b] *National University of Mongolia, Ulan-Bator, 210646 Mongolia*
[c] *RUDN University, Moscow, 117198 Russia*
[d] *Saratov State University, Saratov, 410012 Russia*
[e] *Institute of Nuclear Physics, Almaty, 050032 Kazakhstan*
**e-mail: vinitsky@theor.jinr.ru*

Abstract—New computational schemes, symbolic-numerical algorithms and programs implementing the high-accuracy finite element method (FEM) for the solution of quantum mechanical boundary-value problems (BVPs) are reviewed. The elliptic BVPs in 2D and 3D domains are solved using the multivariable FEM and Kantorovich method using parametric basis functions. We demonstrate and compare the efficiency of the proposed calculation schemes, algorithms, and software by solving the benchmark BVPs that describe the scattering on a barrier and a well, the bound states of a helium atom, and the quadrupole vibration in a collective nuclear model.

DOI: 10.3103/S1062873818060096

INTRODUCTION

Conventionally the elliptic boundary-value problems (BVPs) in multidimensional domains are solved using the multivariable finite element method (FEM) [1]. The alternative Kantorovich method (KM) [2] consists in the expansion of the sought solution over a basis of parametric functions depended on one of the independent variables as a parameter, generated by an appropriate auxiliary eigenvalue problem in a lower-dimension domain. As a result the original BVP is reduced to a set of ordinary second-order differential equations with respect to the above independent variable [3–6]. The computational schemes, symbolic-numerical algorithms and programs implementing the high-accuracy FEM and KM for the solution of quantum mechanical boundary value problems (BVPs) arising in atomic, molecular, and nuclear physics were elaborated [7–10].

In this paper we present a new high-accuracy FEM calculation scheme for solving 2D and 3D scattering problems with *approximated boundary conditions of the third type*. We demonstrate and compare the efficiency of the calculation schemes, algorithms and programs by the examples of solving the benchmark BVPs that describe the quantum scattering by spherical and nonspherical barriers and wells, the bound states of helium atom, and the quadrupole vibration collective nuclear model.

1. THE STATEMENT OF THE PROBLEM

Let us consider of a self-adjoint elliptic partial differential equation (PDE) in the domain $z = (z_1, \ldots, z_d) \in \Omega \subset R^d$ [1]:

$$(D - E)\Phi(z) = \left(-\frac{1}{g_0(z)} \sum_{ij=1}^{d} \frac{\partial}{\partial z_i} g_{ij}(z) \frac{\partial}{\partial z_j} + V(z) - E \right) \Phi(z) = 0, \tag{1}$$

where $g_0(z) > 0$, $g_{ji}(z) = g_{ij}(z)$, and $V(z)$ are real-valued functions, continuous together with their generalized derivatives to a given order. The solution should satisfy the boundary conditions (BC)

$$\begin{aligned} &(\mathrm{I}): \Phi(z)|_S = 0, \ (\mathrm{II}): \left.\frac{\partial \Phi(z)}{\partial n_D}\right|_S = 0, \\ &(\mathrm{III}): \left.\frac{\partial \Phi(z)}{\partial n_D}\right|_S + \sigma(s)\Phi(z)|_S = 0, \end{aligned} \tag{2}$$

$$\frac{\partial \Phi(z)}{\partial n_D} = \sum_{ij=1}^{d} (\hat{n}, \hat{e}_i) g_{ij}(z) \frac{\partial \Phi(z)}{\partial z_j}, \tag{3}$$

where $\partial\Phi(z)/\partial n_D$ is the derivative along the conormal direction, $\hat{n}$ is the outer normal to the boundary $S = \partial\Omega$ of Ω, $\hat{e}_i$ is the unit vector of $z = \sum_{i=1}^{d} \hat{e}_i z_i$, and $(\hat{n}, \hat{e}_i)$ is the scalar product in R^d.

[1] The article is published in the original.

The FEM solution of the BVP is reduced to calculating the stationary points of the Rayleigh–Ritz or Hulten variational functional

$$\Xi(\Phi, E, z) = \int_{\Omega} g_0(z)\Phi^*(z)(D-E)\Phi(z)dz = \Pi(\Phi, E, z) - \oint_S \Phi^*(z)\frac{\partial\Phi(z)}{\partial n_D}ds,$$
$$\Pi(\Phi, E, z) = \int_{\Omega}\left[\sum_{i,j=1}^{d} g_{ij}(z)\frac{\partial\Phi^*(z)}{\partial z_i}\frac{\partial\Phi(z)}{\partial z_j} + g_0(z)\Phi^*(z)(V(z)-E)\Phi(z)\right]dz.$$

For a discrete spectrum problem the functions $\Phi_m(z)$ from the Sobolev space $H_2^{s\geq 1}(\Omega)$, $\Phi_m(z) \in H_2^{s\geq 1}(\Omega)$, corresponding to the real eigenvalues E: $E_1 \leq E_2 \leq \ldots \leq E_m \leq \ldots$ satisfy to the normalization and orthogonality conditions (NOCs)

$$\langle\Phi_m(z)|\Phi_{m'}(z)\rangle = \int_{\Omega} dz g_0(z)\Phi_m(z)\Phi_{m'}(z) = \delta_{mm'},\ dz = dz_1\ldots dz_d. \quad (4)$$

The implementation of high-accuracy multivariate schemes of FEM was considered in [10].

2. QUANTUM SCATTERING PROBLEM FOR BARRIER AND WELL

The 3D BVP (1)–(3) in spherical coordinates (r, θ, φ) with a short-range potential function $V(r, \theta, \varphi) = V(r, \theta)$ at fixed values of the spectral parameter $k^2 = 2mE$ in units $\hbar = m = 1$ is reduced to 2D BVP

$$\left(-\frac{1}{r^2}\frac{\partial}{\partial r}r^2\frac{\partial}{\partial r} - \frac{1}{r^2}\frac{1}{\sin\theta}\frac{\partial}{\partial\theta} \times \sin\theta\frac{\partial}{\partial\theta} + V(r,\theta) - k^2\right)\Psi(r,\theta) = 0 \quad (5)$$

with the boundary conditions

$$\lim_{\theta\to 0,\pi}\sin(\theta)\frac{\partial\Psi(r,\theta)}{\partial\theta} = 0,\ \lim_{r\to 0} r^2\frac{\partial\Psi(r,\theta)}{\partial r} = 0,$$
$$\frac{\partial\Psi(r,\theta)}{\partial r} = R(r,\theta)\Psi(r,\theta),\ r = r_{\max}, \quad (6)$$

where $R(r, \theta)$ is a logarithmic derivative that follows for bounded solutions from the asymptotic boundary conditions

$$\Psi(r,\theta) = \exp(i\vec{k}\vec{r}) + f(\theta)\frac{\exp(ikr)}{r},\ r\to\infty. \quad (7)$$

We rewrite this problem to the inhomogeneous one for the scattering wave $\Phi(r, \theta) = \Psi(r, \theta) - \exp(i\vec{k}\vec{r})$:

$$-\left(\frac{1}{r^2}\frac{\partial}{\partial r}r^2\frac{\partial}{\partial r} + \frac{1}{r^2}\frac{1}{\sin\theta}\frac{\partial}{\partial\theta}\sin\theta\frac{\partial}{\partial\theta}\right) \times \Phi(r,\theta) + (V(r,\theta) - k^2)\Phi(r,\theta) = -V(r,\theta)\exp(i\vec{k}\vec{r}) \quad (8)$$

with the *approximted boundary conditions* that follow from asymptotic BCs (7) for scattered wave

$$\frac{\partial\Phi(r,\theta)}{\partial r} = \left(ik - \frac{1}{r}\right)\Phi(r,\theta),\ r = r_{\max},$$
$$\Phi(r,\theta) = f(\theta)\frac{\exp(ikr)}{r}\left(1 + O\left(\frac{1}{kr}\right)\right),\ r = r_{\max}. \quad (9)$$

Here the unknowns are the scattering wave $\Phi(r, \theta)$ and the amplitude $f(\theta)$. Using the relation for solution $\Phi(r, \theta) = \Psi(r, \theta) - \exp(ikz)$ calculated by means of FEM using the partial S_l-matrix

$$\Phi(r,\theta) = \Psi(r,\theta) - \exp(ikz) = \frac{1}{2i}\sum_{l=0}^{l_{\max}}(2l+1)P_l(\cos\theta)(S_l - 1) \times i^l\{-y_l(kr) + ij_l(kr)\}, \quad (10)$$

where $j_l(r)$ and $y_l(r)$ are the spherical Bessel functions of the first and second kinds, $P_l(\eta)$ are the Legendre polynomials [11], multiplying both sides of Eq. (10) by Legendre polynomials, and integrating over θ, we obtain the required formula for calculating the auxiliary unknown partial S_l-matrix and scattering the amplitude $f_l = (S_l - 1)/(2ik)$:

$$2kf_l = \frac{1}{i}(S_l - 1) = \{i^l(-y_l(kr) + ij_l(kr))\}^{-1} \times \int_0^{\pi}\Phi(r,\theta)P_l(\cos\theta)\sin\theta d\theta,\ l = 0,\ldots,l_{\max}. \quad (11)$$

Using the evaluated values of f_l, we calculate the desired scattering amplitude $f(\theta) = f(\theta, E)$ and the total cross-section $\sigma(E)$ that satisfy the optical theorem

$$f(\theta) = \sum_{l=1}^{l_{\max}}(2l+1)f_lP_l(\cos\theta),$$
$$\sigma(E) = 2\pi\int_0^{\pi}|f(\theta)|^2\sin\theta d\theta = \frac{4\pi}{k}\Im f(\theta = 0). \quad (12)$$

We propose such procedure to consider the contribution of the order $O((kr_{\max})^{-2})$ in the *approximated boundary conditions* (9) and to avoid the use of slowly converging expansion of the *partial boundary conditions* [12, 13]. In the case of a spherical barrier or well, the squared absolute value of the calculated scattering amplitude $f(\theta)$ and its real and imaginary parts at $E = k^2 = 10$, $V(\vec{r}) = \{V_0, r \leq R_0; 0, \text{otherwise}\}$, $R_0 = 1$,

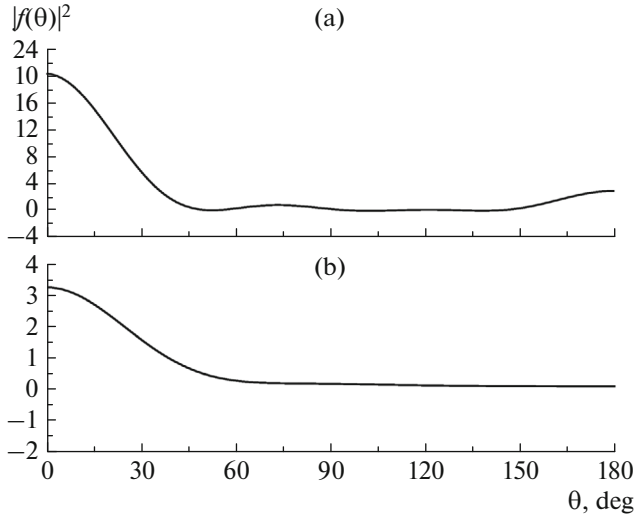

Fig. 1. The absolute square value of the calculated scattering amplitude $f(\theta)$ at $E = k^2 = 10$, for spherical potential $V(\vec{r}) = \{V_0, r \le 1;\ 0,\ \text{otherwise}\}$. (a) $V_0 = 20$, (b) $V_0 = -20$.

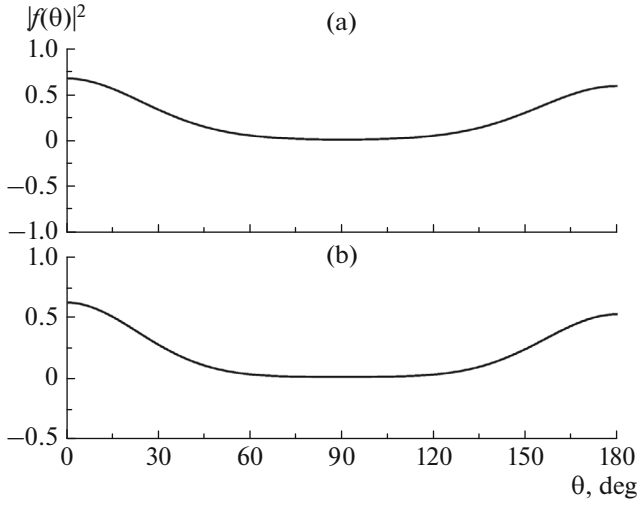

Fig. 2. The same as in Fig. 1 but for nonspherical potential $V(\vec{r}) = \{V_0, r\sin\theta \le 1 \quad \text{and} \quad r|\cos\theta| \le 0.1;\ 0,\ \text{otherwise}\}$. (a) $V_0 = 20$, (b) $V_0 = -20$.

($V_0 = 20$ and $V_0 = -20$) are shown in Fig. 1. The calculation using Eqs. (8), (6), and (9)–(12) was carried out in the 2D domain with the coordinates (r, θ), $\theta \in (0, \pi)$, $r \in (0, r_{\max})$ at $r_{\max} = 100$ on the nonuniform grids $\{0, (60), 3, (100), 50, (100), r_{\max} = 100\}$ and $\{0, (20), \pi\}$, using triangle Lagrange elements of 5th order [10]. The number of mesh points of the *rectangular* grid divided into right-angled triangle elements is indicated in parentheses. The amplitudes calculated from Eqs. (11), (12) at $l_{\max} \approx \sqrt{kr_{\max}}$ are coincided with the accuracy 10^{-5} with exact analytical values, as well as the optical theorem, i.e. w.r.t. of the second Eq. (12).

Similar results for the nonspherical barrier (having the shape of a semitransparent disc of finite thickness) or well $V(\vec{r}) = \{V0,\ \rho = r\sin\theta \le R_0 \text{ and } |z| = r|\cos\theta| \le a/2;\ 0, \text{otherwise}\}$, $R_0 = 1$, $a = 0.2$ are shown in Fig. 2. The calculation was carried out on the nonuniform grids {0, (50), 1, (10), R_1, (100), 50, (100), $r_{\max} = 100$} and {0, (10), φ, (10), π − φ, (10), π} and $\varphi = \arctan\left(R_0/(2a)\right)$, $R_1 = R_0/\sin\varphi$. The optical theorem is implemented with the accuracy 10^{-3}. The obtained results are in a good agreement with the 2D finite difference calculations of Ref. [14].

3. BENCHMARK CALCULATIONS OF HELIUM ATOM BOUND STATES

In the hyperspheroidal coordinates, $0 \le R < \infty$, $1 \le \xi < \infty$, $-1 \le \eta \le 1$, related to the perimetric ones as

$$r_{12} = \frac{\sqrt{2}R}{\sqrt{\xi^2 + \eta^2}},\ r_1 = \frac{R(\xi + \eta)}{\sqrt{2}\sqrt{\xi^2 + \eta^2}},\ r_2 = \frac{R(\xi - \eta)}{\sqrt{2}\sqrt{\xi^2 + \eta^2}}, \tag{13}$$

the equation for the solution $\Psi(R, \xi, \eta) = \sqrt{\xi^2 + \eta^2}\Phi(R, \xi, \eta)$ for S-states of the helium atom (ignoring the negligible effect of electron reduced mass) in atomic units (a.u.) reads as [6]

$$\left[-\frac{1}{R^5}\frac{\partial}{\partial R}R^5\frac{\partial}{\partial R} - \frac{3}{R^2} + \frac{1}{R^2}\frac{(\xi^2 + \eta^2)^2}{\xi^2 - \eta^2} \times\ h(\xi, \eta; R) - 2E\right]\Phi(R, \xi, \eta) = 0, \tag{14}$$

$$h(\xi, \eta; R) = -\frac{\partial}{\partial\xi}(\xi^2 - 1)\frac{\partial}{\partial\xi} - \frac{\partial}{\partial\eta} \times (1 - \eta^2)\frac{\partial}{\partial\eta} + \frac{\sqrt{2}R\left(\xi^2 - \eta^2 - 8\xi\right)}{\sqrt{\xi^2 + \eta^2}^3}. \tag{15}$$

The function $\Phi(R, \xi, \eta)$ satisfies the boundary conditions

$$\lim_{R\to 0} R^5\frac{\partial\Phi(R, \xi, \eta)}{\partial R} = 0,\ \lim_{R\to\infty} R^5\Phi(R, \xi, \eta) = 0, \tag{16}$$

$$\lim_{\xi\to 1}(\xi^2 - 1)\frac{\partial\Phi(R, \xi, \eta)}{\partial\xi} = 0,\ \lim_{\xi\to\infty}\Phi(R, \xi, \eta) = 0,\ \lim_{\eta\to\pm 1}(1 - \eta^2)\frac{\partial\Phi(R, \xi, \eta)}{\partial\eta} = 0 \tag{17}$$

and is normalized by the condition (4) with $g_0(z) = g_0^{(1)}(R)g_0^{(2)}(\xi, \eta)$, $g_0^{(1)}(R) = 8\pi^2R^5$, $g_0^{(2)}(\xi, \eta) =$

$(\xi^2-\eta^2)/(\xi^2+\eta^2)^2$. The parametric surface functions $\phi_i \equiv \phi_i(\xi,\eta;R)$ and the eigenvalues $\varepsilon_i(R)$ are eigensolutions of the 2D BVP with purely discrete spectrum that satisfy the following boundary conditions (17) and the NOC

$$\left[h(\xi,\eta;R)-\varepsilon_i(R)\frac{\xi^2-\eta^2}{(\xi^2+\eta^2)^2}\right]\phi_i=0,$$
$$\langle\phi_i|\phi_j\rangle=\int_1^\infty d\xi\int_{-1}^1 d\eta\,\frac{\xi^2-\eta^2}{(\xi^2+\eta^2)^2} \quad (18)$$
$$\times\,\phi_i(\xi,\eta;R)\phi_j(\xi,\eta;R)=\delta_{ij}.$$

The 2D BVP (18) was solved using the scaled variable and parametric surface functions

$$\xi=\frac{1+\lambda}{1-\lambda},\ 0\le\lambda<1,$$
$$\phi_i(\xi,\eta;R)=\frac{p_i(\xi,\eta;R)}{\xi+1}\equiv\frac{p_i(\lambda,\eta;R)}{\xi+1}. \quad (19)$$

As an example, the potential curves $E_j(R)=(\varepsilon_j(R)-3)/R^2$ and the matrix elements given by the integrals

$$Q_{ij}(R)=-\left\langle\phi_i(\xi,\eta;R)\left|\frac{\partial\phi_j(\xi,\eta;R)}{\partial R}\right.\right\rangle,$$
$$H_{ij}(R)=\left\langle\frac{\partial\phi_i(\xi,\eta;R)}{\partial R}\left|\frac{\partial\phi_j(\xi,\eta;R)}{\partial R}\right.\right\rangle \quad (20)$$

are presented in Fig. 3. The calculations were carried out by means of the program POTHEA 2.0 using the server 2x4 kernels i7k (i7-3770K 4.5 GHz, 32 GB RAM, GPU GTX680), and the Intel Fortran compiler 17.0. The computing time per one point R for the considered examples with the accuracy 10^{-12} with triangular Lagrange elements of the 5th order on the uniform 2D grids $\lambda=\{0(L)1\}$, $\eta=\{0(L)1\}$ at $L=10,20,40$ was 0.38, 5.08, and 41.21 seconds, respectively [10]. We seek for the solution of the 3D BVP (14)–(17) expressed as the Kantorovich expansion [2]

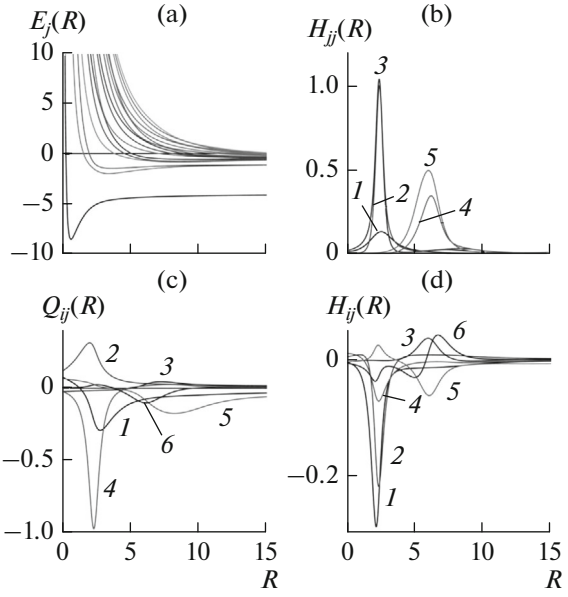

Fig. 3. (a) Potential curves $E_i(R)$, $i=1,...,16$. The matrix elements (b) $H_{jj}(R)$ ((*1*) $H_{11}(R)$, (*2*) $H_{22}(R)$, (*3*) $H_{33}(R)$, (*4*) $H_{44}(R)$, (*5*) $H_{55}(R)$), (c) $Q_{ij}(R)$ ((*1*) $Q_{12}(R)$, (*2*) $Q_{13}(R)$, (*3*) $Q_{14}(R)$, (*4*) $Q_{23}(R)$, (*5*) $Q_{24}(R)$, (*6*) $Q_{34}(R)$) and (d) $H_{ij}(R)$ ((*1*) $H_{12}(R)$, (*2*) $H_{13}(R)$, (*3*) $H_{14}(R)$, (*4*) $H_{23}(R)$, (*5*) $H_{24}(R)$, (*6*) $H_{34}(R)$) plotted vs hyperradius R (in a.u.).

$$\Phi(R,\xi,\eta)=\sum_{j=1}^{j_{\max}}\phi_j(\xi,\eta;R)\chi_j(R) \quad (21)$$

over the eigenfunctions $\phi_j(\xi,\eta;R)$ of the parametric 2D BVP having the purely discrete spectrum $E_j(R)=(\varepsilon_j(R)-3)/R^2$, $j=1,2,....$ Substituting the expansion (21) into the 3D BVP Eqs. (14)–(17), we get the 1D BVP for a finite set of $j_{\max}$ coupled ordinary differential equations for $\boldsymbol{\chi}(R)=\{\chi_1(R),...,\chi_{j_{\max}}(R)\}^{\mathrm{T}}$

$$\left(-\frac{1}{R^5}\mathbf{I}\frac{d}{dR}R^5\frac{d}{dR}+\mathbf{V}(R)+\mathbf{Q}(R)\frac{d}{dR}+\frac{1}{R^5}\frac{dR^5\mathbf{Q}(R)}{dR}-2E_m\mathbf{I}\right)\boldsymbol{\chi}_m(R)=0, \quad (22)$$

where $\mathbf{I}$ is unit matrix of dimension $j_{\max}\times j_{\max}$, $\mathbf{V}(R)=\mathbf{H}(R)+\mathbf{E}(R)$ and $\mathbf{Q}(R)$ are matrices of dimension $j_{\max}\times j_{\max}$ given by their matrix elements (20) with the boundary and normalization conditions

$$\lim_{R\to0}R^5\frac{d\boldsymbol{\chi}_m(R)}{dR}=0,\ \lim_{R\to\infty}R^5\boldsymbol{\chi}_m(R)=0,$$
$$8\pi^2\int_0^\infty dR R^5(\boldsymbol{\chi}_m(R))^{\mathrm{T}}\boldsymbol{\chi}_{m'}(R)=\delta_{mm'}. \quad (23)$$

The solution of this BVP with the help of KANTBP program [9] on the non-uniform grids $R=\{0(50),5,(75),20\}$ using the calculated $E_j(R)$, $V_{ij}(R)=H_{ij}(R)+E_j(R)\delta_{ij}$, $Q_{ij}(R)$, $i,j=1,...,12$, i.e. using 12 surface basis functions, yields the upper estimate for the energy of the ground and the first exited state of helium atom $E_1=-2.90372430$ a.u. and $E_2=-2.14597322$ a.u. with 8 significant digits, similar to the results of the POTHEA program with 28 basis functions [8]. The first three components of

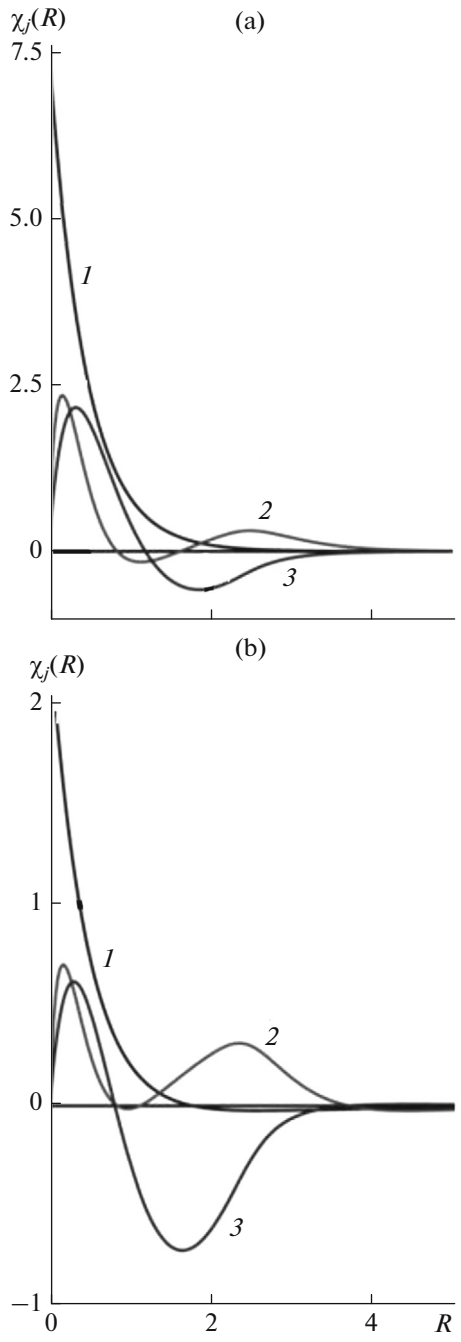

Fig. 4. The first three components of the radial eigenfunctions $\chi_j(R)$ of ground (a) and first exited (b) states of helium atom plotted vs hyperradius R (in a.u.) ((*1*) $\chi_1(R)$, (*2*) $\chi_2(R),10^{-2}$, (*3*) $\chi_3(R),10^{-2}$).

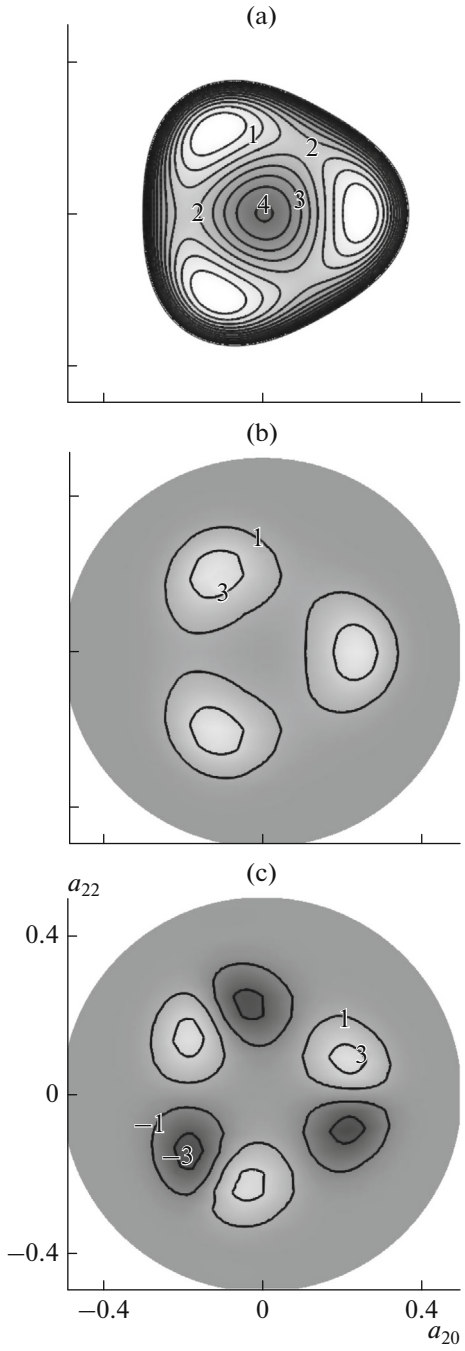

Fig. 5. (a) The isolines of potential energy of quadrupole shape (24) (in MeV) and two non-degenerated eigenfunctions (b) Φ_1 and (c) Φ_6.

the radial eigenfunctions of the ground and the first exited states of helium atom vs the hyperradius R are plotted in Fig. 4. One can see that the absolute values of the components decrease with the increase of their numbers, which clearly demonstrates the convergence rate of KM (21).

4. VIBRATIONAL COLLECTIVE C_{3v} QUADRUPOLE NUCLEAR MODEL

Let us consider the 2D BVP described by Eqs. (1), (2), and (4) for $x = a_{22}$, $y = a_{20}$ with the potential function $U(x,y) = 2mV(x,y)$ and the spectral parameter $\varepsilon = 2mE$, and $g_0(x,y) = g_{ij}(x,y) = 1$. The quad-

Table 1. The first energy levels of the 2D BVP using triangular ε_i^{Δ} and rectangular $\varepsilon_i^{\square}$ finite elements and the KM ε_i using $j_{\max} = 28$ parametric basis functions, classified by irrs (Class.) of the C_{3v} point group, E_i (MeV)

i	ε_i^{Δ}	$\varepsilon_i^{\square}$	ε_i	$E_i = \varepsilon_i/2m$	Class.
1	381.754344	381.754355	381.754351	1.53933206	A1
2	387.240633	387.240644	387.240641	1.56145419	E1
3	387.240633	387.240646	387.240641	1.56145419	E2
4	617.024951	617.024967	617.024963	2.48800388	E1
5	617.024951	617.024989	617.024963	2.48800388	E2
6	667.104970	667.105020	667.104992	2.68993948	A2
7	695.166557	695.166590	695.166575	2.80309103	A1
8	785.680037	785.680100	785.680078	3.16806483	E1
9	785.680037	785.680136	785.680078	3.16806483	E2
10	898.045395	898.045497	898.045434	3.62115094	A1
11	915.823095	915.823200	915.823167	3.69283535	E1
12	915.823095	915.823309	915.823167	3.69283535	E2
13	993.158636	993.158784	993.158708	4.00467221	E2
14	993.158636	993.158872	993.158708	4.00467221	E1
15	1063.73690	1063.73709	1063.73692	4.28926178	A1

rupole potential energy is approximated by the quartic potential [5]:

$$V(a_{22},a_{20}) = c_1(a_{22}^2 + a_{20}^2) + c_2(a_{22}^2 a_{20} - a_{20}^3/3) + c_3(a_{22}^2 + a_{20}^2)^2 + c_0. \quad (24)$$

We use the set of parameters $c_1 = -120$, $c_2 = 240$, $c_3 = 1200$, $c_0 = 65/16$ that provide a crude approximation for the shape of $^{156}_{64}\mathrm{Gd}_{92}$, which has been fitted in the following points: the minima at $(a_{22},a_{20}) = (0,1/4)$, $V(0,\ 1/4) = 0$; the maxima at $(a_{22},a_{20}) = (0,0)$, $V(0,0) = 65/16$; and the saddle point at $(a_{22},a_{20}) = (0,-1/5)$, $V(0,\ 1/5) = 729/400$ (see Fig. 5). The fitting points in our parametrization are related to those of Ref. [15] as $a_{22} = \sqrt{2}\alpha_{22}$, $a_{20} = \alpha_{20}$. We choose the effective mass parameter to be $m = B_2 = 124$. Thus, there are ground and doubly degenerate excited states, localized in three wells. The point symmetry group C_{3v} of the 2D problem (1), (2), (4), (24) has four irreducible representations (irrs.) A1, A2, E1 and E2 to classify the solutions, the E-type states being doubly degenerate [16]. The calculated eigenvalues are presented in Table 1. The first eigenfunctions of the irrs. A1, A2 are shown in Fig. 5. The BVP was solved using four ways:

(1) The solution of the 2D BVP was calculated using the FEM scheme on the *rectangular* grid $[-0.4,-0.3,...,0.4] \times [-0.4,-0.3,...,0.4]$ with Lagrange interpolation polynomials of the order $p = 12$. The first 15 eigenvalues were calculated with 9 significant digits and are presented in Table 1.

(2) In the solution of the 2D BVP we used 54 finite elements in the form of *equilateral triangles* with the side equal to 1/6, forming a regular hexagon with the vertices $\{(0.5\cos\pi n/3,\ \ 0.5\sin\pi n/3)\}_{n=0}^{5}$. In each finite element the Lagrange interpolation polynomials of the fifth order were applied [10]. The stiffness and the mass 721×721 matrices were used. The calculated eigenvalues are presented in Table 1. The results ε_i^{Δ} of the above FEM calculations give upper estimations of $\varepsilon_i^{\square}$ for first 15 eigenvalues.

(3) The 2D problem (1), (2), (4), (24) was also solved using the KM implemented in the FEM program KANTBP 3 [9], with $j_{\max}$ 28 parametric basis functions of one of the independent variables as a parameter, calculated using the FEM program ODPEVP [7]. The solution was calculated in the domain $\sqrt{a_{20}^2 + a_{22}^2} < 1/2$ with Dirichlet BCs at the boundary $\sqrt{a_{20}^2 + a_{22}^2} = 1/2$ using the calculation scheme similar to KM presented in Section 3. The calculations were performed on the finite element grid $\{-1/2, -1/3, -1/6, 0, 1/3, 1/2\}$ with Lagrange interpolation polynomials of the order $p = 12$. The results ε_i^{Δ} and $\varepsilon_i^{\square}$ of the above FEM calculations give upper and lower estimations of ε_i, respetively.

(4) We performed also the calculations using KM with parametric basis function given in analytical form [5]. The results coincide with those of the calculations of ε_i presented in Table 1 with 9 significant digits.

CONCLUSIONS

The proposed calculation schemes, algorithms and software implemented the high-accuracy finite element method and Kantorovich method for solving the boundary value problems can be applied to analyze the dynamics of few-body scattering problems, quantum tunneling and diffraction models, and quantum scattering by nonspherical objects and nuclei.

ACKNOWLEDGMENTS

The authors thank Prof. A. Góźdź and Prof. F.M. Pen'kov for collaboration. The work was supported partially by the RFBR (grant nos. 16-01-00080 and 18-51-18005), the RUDN University Program 5-100, the grant MES RK 0333/GF4, and grant of Plenipotentiary Representative of the Government of the Republic of Kazakhstan in the framework of collaboration program JINR-RK N 337 2017.

REFERENCES

1. Ciarlet, P., *The Finite Element Method for Elliptic Problems*, Amsterdam: North-Holland, 1978.
2. Kantorovich, L.V. and Krylov, V.I., *Approximate Methods of Higher Analysis*, New York: Wiley, 1964.
3. Vinitsky, S.I., Gusev, A.A., Chuluunbaatar, O., et al., *Lect. Notes Comput. Sci.*, 2014, vol. 8660, p. 472.
4. Gusev, A.A., Vinitsky, S.I., Chuluunbaatar, O., Hai, L.L., Derbov, V.L., Góźdź, A., and Krassovitskiy, P.M., *Phys. At. Nucl.*, 2014, vol. 77, p. 389.
5. Gusev, A.A., Vinitsky, S.I., Góźdź, A., et al., *Acta Phys. Pol. B Proc. Suppl.*, 2017, vol. 10, p. 99.
6. Vinitsky, S.I., Gusev, A.A., Chuluunbaatar, O., et al., *Proc. SPIE*, 2016, vol. 9917, p. 99172Z1.
7. Chuluunbaatar, O., Gusev, A.A., Vinitsky, S.I., and Abrashkevich, A.G., *Comput. Phys. Commun.*, 2009, vol. 180, p. 1358.
8. Gusev, A.A., Chuluunbaatar, O., Vinitsky, S.I., and Abrashkevich, A.G., *Comput. Phys. Commun.*, 2014, vol. 185, p. 2636.
9. Gusev, A.A., Chuluunbaatar, O., Vinitsky, S.I., and Abrashkevich, A.G., *Comput. Phys. Commun.*, 2014, vol. 185, p. 3341.
10. Gusev, A.A., Gerdt, V.P., Chuluunbaatar, O., et al., *Lect. Notes Comput. Sci.*, 2017, vol. 10490, p. 134; Gusev, A.A., Gerdt, V.P., Chuluunbaatar, O., et al., *Lect. Notes Comput. Sci.*, 2017, vol. 10490, p. 151.
11. Abramowitz, M. and Stegun, I.A., *Handbook of Mathematical Functions*, New York: Dover, 1965.
12. Konyaev, D.A. and Delitsyn, A.L., *Mat. Model.*, 2014, vol. 26, no. 8, p. 48.
13. Delitsyn, A.L., *Moscow Univ. Phys. Bull.*, 2017, vol. 72, p. 340.
14. Krassovitskiy, P.M. and Pen'kov, F.M., *Bull. Russ. Acad. Sci.: Phys.*, 2017, vol. 81, p. 730.
15. Dobrowolski, A., Mazurek, K., and Góźdź, A., *Phys. Rev. C*, 2017, vol. 94, p. 054322.
16. Cornwell, J.F., *Group Theory in Physics*, New York: Academic, 1984.